Hydroxyl-stretching region in the Raman broad scans on minerals of the vivianite group

Amelia Carolina Sparavigna

Department of Applied Science and Technology, Polytechnic University of Turin, Italy

amelia.sparavigna@polito.it

Vivianite is a hydrated iron phosphate mineral ($Fe_3(PO_4)_2 \cdot 8H_2O$), crystallized in a monoclinic system. It is the endmember of a mineral series known as the vivianite group, where minerals have the general formula $A_3(XO_4)_2 \cdot 8H_2O$, A is a divalent metal cation and X is phosphorus P or arsenic As. Today, vivianite is attracting interest as a promising material for recovering phosphorous from wastewaters. In fact, the presence in wastewater sludges of soluble iron and phosphorus can lead to vivianite formation. As a crystal, it is a naturally occurring Van der Walls material. It can be easily characterized by means of Raman and infrared spectroscopies. Here we will consider the Raman spectroscopy, precisely that related to the hydroxyl-stretching region. We will propose the deconvolutions in q-Gaussian functions of spectra from RRUFF database, comparing the obtained results with those available from literature. Besides vivianite, we will consider also baricite and bobierrite for comparison (baricite and bobierrite are two other members of the vivianite group). About the hydroxyl-stretching region and the use of q-Gaussians, we take the chance to continue a discussion regarding the Raman spectroscopy of water, discussion that we started in March 2024.

Keywords: Vivianite group minerals, Vivianite, Baricite, Bobierrite, Raman spectroscopy, q-Gaussian functions, Hydroxyl-stretching Raman region.

Introduction - Here we consider the Raman broad scans on minerals of the vivianite group, which are kindly offered by the RRUFF database. The minerals of the vivianite group are of the general formula $A_3^{2+}(XO_4)_2 \cdot 8H_2O$. In this formula, A^{2+} can be Co, Fe, Mg, Ni, Zn and X can be As or P (Frost et al., 2002). In RRUFF database, we can find vivianite, baricite, bobierrite and other minerals of the group. Of the Raman broad scans we will consider the range between 2000 and 4000 cm^{-1}, which contains the hydroxyl-stretching region (for water, from 2800 to 3800 cm^{-1}). We have already considered this region when we studied the Raman spectroscopy of water; we proposed specifically the decomposition of this large OH stretching Raman band in components with the q-Gaussian profiles. Being the q-parameter of q-Gaussian functions related to the correlation time of stochastic Kubo modelling of fluctuations, we stressed the use of this parameter to characterize the local environments of O-H bonds. We further discussed the OH-stretching band of ice, to understand how the decomposition in q-Gaussians changes in the number of components and values of q-parameters. Here, besides discussing vivianite OH- stretching band, we will propose a further analysis of the Raman spectroscopy on water, to stress the crucial points of it. We will apply the same approach used for water, that is a decomposition of the spectrum in q-Gaussian components, to the scans on vivianite. We will compare the results obtained by means of q-Gaussians with the results given by literature. Baricite and bobierrite are also studied.

Before addressing the Raman spectroscopy of Vivianite, let us remember some general literature about this material.

Literature about vivianite - In Frisenda et al., 2020, we can find discussed the *naturally occurring van der Waals materials*. Among the phosphates, Frisenda and coworkers described the vivianite as "a hydrated iron phosphate with an approximate formula $Fe^{2+}Fe_2^{2+}(PO_4)_2 \cdot 8H_2O$. Vivianite is known to be sensitive to visible light exposure which leads to a marked change in its color from colorless/pale green to dark green/brown. Bulk vivianite has been used as natural electron donor to effectively dechlorinate a variety of chlorinated organics, the principal and most frequently found contaminants in soil and groundwater that generates significant environmental problems". Frisenda and coworkers also provide references about the band gap of vivianite as "an indirect band gap in the range of ~3.3–4.6 eV and a paramagnetic ground state" (Li et al., 2016, Pinto et al., 2014).

About vivianite we have a large literature on its natural occurrences in different environmental conditions. Rothe and coworkers, 2016, proposed a review of "the nature, occurrence and environmental relevance of" vivianite. As explained by Silva et al., 2024, vivianite is a "mineral that can be associated with biogeochemical processes. The mineral is found in freshwater and marine systems as a biogenic product while it can undergo oxidation caused by the action of neutrophilic or photoautotrophic microorganisms" (Silva et al., mentioning Rothe et al., 2016, Miot et al., 2009, Kappler & Newman, 2004). For a recent review, see Paskin, 2024.

In industrial environment, v*ivianite can be found in wastewater treatment plants*. As noted in Prot et al., 2021, the presence in wastewater sludge of soluble iron and phosphorus can lead to vivianite formation, that is to the "vivianite scaling" problem. "Vivianite scaling is widely occurring in wastewater treatment plant even though it is rarely reported". "Iron reduction appears to be the cause of vivianite scaling in anaerobic equipment. … Solubility of vivianite decreases when T>32 °C, favoring scaling in heat exchangers. … [Vivianite] is usually present as a hard and blue deposit that can also be brown or black depending on its composition and location" (Prot et al., 2021). However, vivianite can be turned into an important resource; this can happen by means of methods for the phosphorus recovery (Yang et al., 2023).

In Wu et al., 2019, we can find a review of "potentials and challenges of phosphorus recovery as vivianite from wastewater". "Due to the shortage of phosphorus resources and the limitations of existing phosphorus recovery methods, phosphorus recovery in the form of vivianite has attracted considerable attention with its natural ubiquity, easy accessibility and foreseeable economic value". Wu and coworkers are proposing a review which summarizes the chemistry of vivianite. Then, "the potential of phosphorus recovery as vivianite from wastewater has also been comprehensively examined from the prospects of economic value and engineering feasibility. … However, the insufficient understanding on vivianite recovery in wastewater/sludge decelerate the development and exploration of such advanced approach" (Wu et al., 2019).

Zhang et al., 2022, note that the development of "feasible techniques to recover phosphorous (P) from wastewater and sewage sludge is urgent work to meet the huge demand for P resources and wastewater/sludge management. Recently, recovering P as value-added vivianite has aroused great interest due to the convenient process operation, high recovery efficiency, and wide applications of vivianite". Advanced technologies are "including ion exchange, electrodialysis, capacitive de-ionization, membrane bioreactor, anaerobic fermentation, chemical precipitation, electrochemical crystallization, biomineralization, and anaerobic digestion" as summarized by Zhang and coworkers.

Other literature on this subject, that is the sewage and wastewater treatment, are Wilfert et al., 2016, 2018, Liu et al., 2018, Wang et al., 2018. Zhao et al., 2024, propose an "efficient phosphorus recovery from waste activated sludge", by means of a "pretreatment with natural deep eutectic solvent and recovery as vivianite". Lu et al., 2024, study the "anaerobic recovery of vivianite from waste-

activated sludge through combined sludge pre-fermentation and agroforestry biomass-based biochar". "If enough iron is present in the sludge after anaerobic digestion, 70–90% of total phosphorus (P) can be bound in vivianite. Based on its paramagnetism and inspired by technologies used in the mining industry, a magnetic separation procedure has been developed" (Prot et al., 2019).

Lu and coworkers stress that phosphorus "plays a crucial role in the growth of plants and crops", "but the utilization of phosphorus resources faces two significant challenges. On the one hand, under natural conditions, phosphorus ore is non-renewable". According to Lu and coworkers, we are therefore facing a "phosphorus crisis" in human society. Since "phosphorus is easily discharged into the water through human production and daily life", we are at the same time facing a "phosphorus pollution" (see Lu et al, and references therein). Lu and coworkers are providing references about the applications of vivianite, "particularly in producing high-value products like lithium batteries" (Lu et al., mentioning Wang et al., 2023, "the obtained vivianite can be used to produce high value-added products such as lithium batteries"). Moreover, vivianite "can be efficiently synthesized during the anaerobic fermentation of waste-activated sludge (WAS)". Lu and coworkers concentrate the research on the use of carbonaceous materials in vivianite formation; the researchers mention graphite, carbon nanotubes, and biochar, "as a more affordable, easily produced, and sustainable carbon material, [which] holds significant potential in accelerating electron transfer processes" (Lu et al., and references therein). Therefore, "understanding the vivianite synthesis system's response mechanisms after adding biochar is crucial for improving the efficiency of vivianite formation". About biochar, see Sparavigna and references therein.

"As an important product of extracellular electron transfer (EET) and biological iron reduction, the production of vivianite can be enhanced by conductive materials. Carbon nanotubes (CNTs) with excellent electrical conductivity have been reported to promote electron transfer, which was applied in wastewater treatment to accelerate the degradation of the contaminants" (He et al., 2022). He and coworkers studied the influence of carbon nanotubes CNTs in vivianite production. "The enhancement of vivianite production after CNTs adding reached up to 17 % by promoting the electron transfer between dissimilative iron-reducing bacteria (DIRB) and Fe(III)".

Vivianite uses - A description of vivianite uses is given by geologyin.com .

Vivianite has scientific uses. It is an *environmental indicator*: "Vivianite's presence in sediments can reveal past environmental conditions, including oxygen levels, pH, and the availability of iron and phosphorus. This information aids in reconstructing paleoclimate and understanding past ecological changes". It is a *geochemical tracer*: "Researchers studying the transportation and fate of iron and phosphorus in aquatic environments can utilize vivianite as a natural tracer due to its specific formation conditions and reactivity". Vivianite is a *paleontological tool*: "Fossilized vivianite alongside fossils of organisms like fish or plants can provide insights into ancient ecosystems and the interactions between organisms and their environment. Besides the scientific uses, we have the use of vivianite as a gemstone and for mineral collection. The web site is also mentioning the vivianite *cultural use*, with associated symbolic values.

Vivianite in the News - "Wastewater: recover vivianite mineral, from lab to pilot scale - with Wetsus partner", 05/12/2023, https://www.water4all-partnership.eu/news/wastewater-recover-vivianite-mineral-lab-pilot-scale-wetsus-partner

"Siderite and Vivianite as Energy Sources for the Extreme Acidophilic Bacterium Acidithiobacillus Ferrooxidans in the Context of Mars Habitability", by Keith Cowing, Status Report, Nature, July 1, 2024, https://astrobiology.com/2024/07/siderite-and-vivianite-as-energy-sources-for-the-extreme-acidophilic-bacterium-acidithiobacillus-ferrooxidans-in-the-context-of-mars-habitability.html This Status Report is referring to the article by Silva et al., 2024.

"L'utilizzo della vivianite per ridurre la clorosi ferrica su olivo", Teatro Naturale, 03/05/2024, https://www.teatronaturale.it/strettamente-tecnico/l-arca-olearia/42200-l-utilizzo-della-vivianite-per-ridurre-la-clorosi-ferrica-su-olivo.htm

"Study on anaerobic phosphorus release from pig manure and phosphorus recovery by vivianite method", by Chen et al., 2023, https://www.nature.com/articles/s41598-023-43216-5

"Mineral Monday: Vivianite. This week, learn about the spectacular mineral vivianite", June 04, 2018, by Jennifer Theresa Kent, https://www.unr.edu/nevada-today/news/2018/mineral-monday-vivianite

"Improving phosphorus recycling from sewage sludge", "Doctoral student Lena Heinrich also took her samples at the Münchehofe wastewater treatment plant to study the formation of vivianite", 24/10/2022, https://smartwatermagazine.com/news/forschungsverbund-berlin-ev/improving-phosphorus-recycling-sewage-sludge

"Des Moines' sewer pipe crud cited for its beauty", May 24, 2023, News by Jason Clayworth, https://www.axios.com/local/des-moines/2023/05/24/sewer-pipe-crud-desmoines-art-beauty-wastewater

"Vivianite blues", by Caroline P. Slomp, Nature. "From Dutch painters to ocean sediments, Caroline Slomp discusses the role vivianite plays in the distribution of phosphorus, an essential nutrient for life". 11 May, 2023, https://www.nature.com/articles/s41561-023-01174-7

Structure - "In pure end member vivianite all the iron is divalent, Fe^{2+}, but there are two distinct sites in the structure that these ions can occupy. In the first site, the Fe^{2+} is surrounded by four water molecules and two oxygens, making an octahedral group. In the second site, the Fe^{2+} is surrounded by two water molecules and four oxygens, again making an octahedral group. The oxygens are part of the phosphate groups (PO_4^{3-}), that are tetrahedral. The vivianite structure has chains of these octahedra and tetrahedra that form sheets perpendicular to the a-crystal axis. The sheets are held together by weak bonds, and that accounts for the perfect cleavage between them" (Wikipedia, mentioning Pring, 1998).

IR and Raman spectroscopy - Paskin, 2024, tells that infrared and Raman spectroscopy are helpful in vivianite identification. "The IR spectrum of vivianite shows characteristic H-O-H stretching and bending modes at nearly 3430 cm^{-1} and 1690 cm^{-1} respectively, the tetrahedral phosphate group shows vibrations at 974 – 1037 cm^{-1}. … . An advantage of using Raman spectroscopy over IR is that data below 400 cm^{-1} can be obtained. Vivianite shows strong broad O-H stretching bands between 3000 to 3700 cm^{-1} . The strongest band in the Raman spectrum is at 3262 cm^{-1} attributable to the OH stretching. A strong band is observed at 951 cm^{-1} and is due to the Raman active PO stretching. Two intense bands are observed at 236 and 186 cm^{-1} and these bands are attributable to Fe-O stretching vibrations" (Paskin mentioning Frost et al., 2002)

.

Raman spectrum according to Frost et al., 2002, and Ogorodova et al., 2017 - In the article by Frost and coworkers, 2002, we can find the Raman and IR spectra of vivianite, baricite and bobierrite in their Figures 1 and 2. The analysis of the Raman and IR spectra are reported in Table 1 of their article. In the following Table I, we consider only the Raman bands (cm^{-1}), as in the Figure 1 in Frost et al., 2002.

Table I (centers of the bands, cm^{-1})

Vivianite	Baricite	Bobierrite	
3496	3480	3498	Assignment
3482	3300	3263	proposed
3262	3231	3212	
3130	3121	3096	Hydroxyl
3012	3025	2895	stretching

"Vivianite shows well-resolved bands in the hydroxyl-stretching region at 3496, 3482, 3262, 3130 and 3012 cm^{-1}" (Frost et al., 2002). "The band at 3262 cm^{-1} is most intense in the Raman spectrum and is assigned to the water *OH symmetric stretching* mode". "The Raman spectra of both baricite and bobierrite are less well resolved than that of vivianite, although the spectral profiles are similar". The instrument used by Frost and coworkers is a Renishaw 1000 Raman. The Raman spectra were excited by a He-Ne laser (633 nm). "Repeated acquisitions using the highest magnification were accumulated to improve the signal to noise ratio in the spectra". "Spectra at liquid nitrogen temperature were obtained using a Linkam thermal stage". "Band-component analysis was undertaken using the Jandel 'Peakfit' software package, … Band fitting was done using a Gauss-Lorentz cross-product function with the *minimum number of component bands used to achieve a satisfactory fit*. The Gauss-Lorentz ratio was maintained at values *greater than 0.7*". The Gauss-Lorentz cross product functions are not given in the article by Frost et al.; in Origin Help we find an expression which is governed by parameter "s" as shape. Probably, the "ratio" in Frost et al. is the "shape" in Origin. In the Table I given by Frost and coworkers, four bands are given, but in the Figure 1 of the same article, the components used for fitting are five.

In Ogorodova et al., 2017, we can find in the Figure 3 a Raman spectrum of vivianite. "Raman spectroscopic study was carried out on a Raman microscope EnSpectr R532 (Russia) with a diffraction grating (1800 lines/mm) and a spectral resolution of about 6 cm^{-1}. The laser radiation wavelength was equal to 532 nm, the laser radiation power on the sample was approximately 15 mW, … Spectrum was obtained on a non-oriented single crystal". "Anion $[PO_4]^{3-}$ is manifested in the spectrum by a group of lines: a strong line at 950 cm^{-1} corresponds to the totally symmetric valence vibration of the anion; a weak line at 1055 cm^{-1} relates to the triply degenerate antisymmetric valence vibration; the lines at 539 and 572 cm^{-1} belong to the triply degenerate deformation vibration; a line near 458 cm^{-1} corresponds to doubly degenerate deformation vibration of tetrahedra $[PO_4]^{3-}$. The high-frequency line with maximum at 3138 cm^{-1} and shoulder near 3280 cm^{-1} correspond to the valence vibrations of OH-groups (in water molecules). A weak line with maximum near 3475 cm^{-1} relates to valence vibrations of OH-groups in the coordination $Fe^{3+}OH$" (Ogorodova et al., mentioning Frost et al., 2004).

In the Figure 3 of the article by Ogorodova et al., we find the peaks at (cm^{-1}):

132 170 198 241 345 458 539 572 624 850 950 1055 1663 3138 3280 3475

In the work by Frost et al., 2004, we find the Raman spectra of several samples of Vivianite. Again, we find that the researchers used PeakFit and Gauss-Lorentzian cross product functions, "with the minimum number of component bands used for the fitting process". The following table contains the centers of the peaks of natural Vivianite samples given by Frost et al. in 2004, plus the centers given in Frost et al., 2002, and those given by Ogorodova et al.

Table II (centers of the bands, cm^{-1})

Chernomorskiy(a)		3137	3268		3487
Blackbird Dist		3131	3247		3473, 3486
Huanuni(a)		3131	3242, 3270, 3272		3480
Monserrat	2958	3133	3262		3478
Chernomorskiy(b)	3031	3137	3253	3351	3493
Huanuni(b)	3010	3135	3257	3391	
Vivianite (2002)	3012	3130	3263		3482, 3496
Ogorodova et al.		3138	3280		3475

We can see that three peaks are always detected. Moreover, the hydroxyl-stretching Raman region seems being composed by five bands in generals.

Frost et al., 2002, wrote that "the band at 3262 cm^{-1} is most intense in the Raman spectrum and is assigned to the water OH symmetric stretching mode". Ogorodova et al., 2017, wrote that "the high-frequency line with maximum at 3138 cm^{-1} and shoulder near 3280 cm^{-1} correspond to the valence vibrations of OH-groups (in water molecules)". Due to these two affirmations, it is necessary to shortly consider the Raman spectrum of water.

Water - In previous discussions, Sparavigna, 2024, we have reviewed literature and proposed the deconvolution of the hydroxyl-stretching region of water and ice with the q-Gaussian functions. For a comparison water/ice we used the Figure 2 in Đuričković et al., 2011. As other researchers did, Đuričković and coworkers noted that the "broad range of the Raman spectrum of liquid water originates from the symmetric and asymmetric OH–stretching vibrations. The fact that this band is rather broad implies the need for its deconvolution into several components, and a large controversy about the number of components and their origins exists in the literature" (Đuričković et al., mentioning Wang et al., 2003). According to the used number of components, researchers established the vibrational mechanisms from intra- and intermolecular bonds (see discussion in Sparavigna, 2024). Let us consider just two components, for instance. We can find them assigned to symmetric and asymmetric vibrations respectively, as in Đuričković et al., 2011. If we use four components, we can find Carey, 1998, saying that these bands are corresponding to four modes due to "the splitting of the v_1 symmetrical stretching vibration into four distinct vibrations".

In our previous discussion about water and ice, we considered two main q-Gaussian components, characterized by two different q-parameters. We proposed the two parameters as linked to two different local environments of OH-bonds (the q-parameters of q-Gaussians can be related to the correlation time of stochastic Kubo modelling of fluctuations). As stressed by Martin Chaplin in his discussion about the vibrational spectra, the "water structuring is now firmly established … as best interpreted using a two-state water mixture" (Chaplin mentioning Gallo et al., 2016). Of course, the two states have a differente local environment for their oscillators.

In Gallo et al., Section 4, we find told that theoretical and experimental results are today modelled by the presence of "two alternative structures" in water, "described as a low- and a high-density liquid". "The anomalies of supercooled water and the possibility of metastable liquid−liquid separation in water can be explained if water is viewed as a mixture of two interconvertible organizations of hydrogen bonds whose ratio is controlled by thermodynamic equilibrium" (Gallo et al., 2016). The water molecules are consequently organized "into two distinct groups: one corresponding to low-energy/low entropy ordered configurations and the other to high-energy/high-entropy configurations. In this picture the complexity of water is thus modeled by a mixture of these two structural motifs" (Gallo et al., 2016).

As previously told, for our deconvolution of the water 3200-3400 cm^{-1} band, we proposed the q-Gaussian functions, which have a shape changing from Lorentzian to Gaussian,according to the q-parameter of the q-exponential Tsallis function (see Appendix). We linked the q-parameter to the local environment of the oscillators. In fact, the approach with q-Gaussians is suitable for a two-fluids model, where each fluid is characterized by a different entropic index. Actually, the q-parameter is the entropic index of the Tsallis entropy.

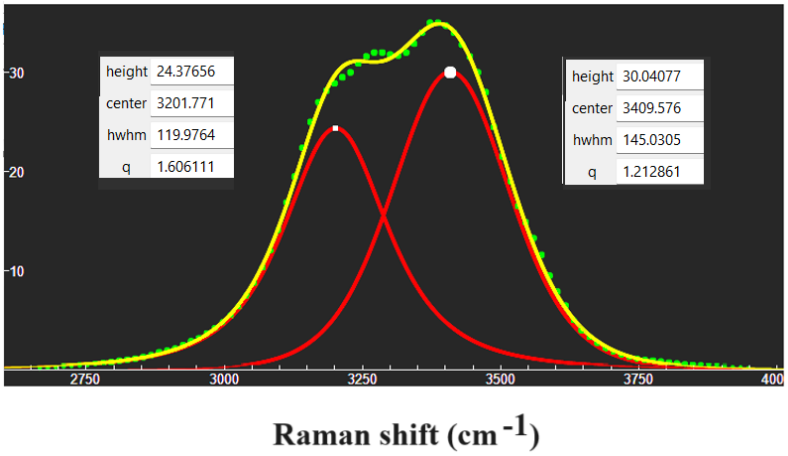

Fig.1: Deconvolution of the OH-stretching band of water, obtained by means of two q-Gaussian functions (red curves). The green dots are representing the data as given by in Đuričković et al., 2011. The yellow line is the sum of components. Parameters of the functions are given close the components. Note the different value of the q-parameters, meaning that oscillators are in two different environments. The plot is obtained with Fityk, after defining in it the q-Gaussians (see Appendix for further details).

Let us consider the data from Đuričković et al., 2011, and make a fit with two q-Gaussians (Fig.1). We can clearly see that the two q-Gaussians have different q-parameters, and consequently two different Tsallis entropic indexes (again, we can argue that the different entropic indexes are due to two different local environments with two different entropies). We can improve the fit, adding two further small components (Fig.2).

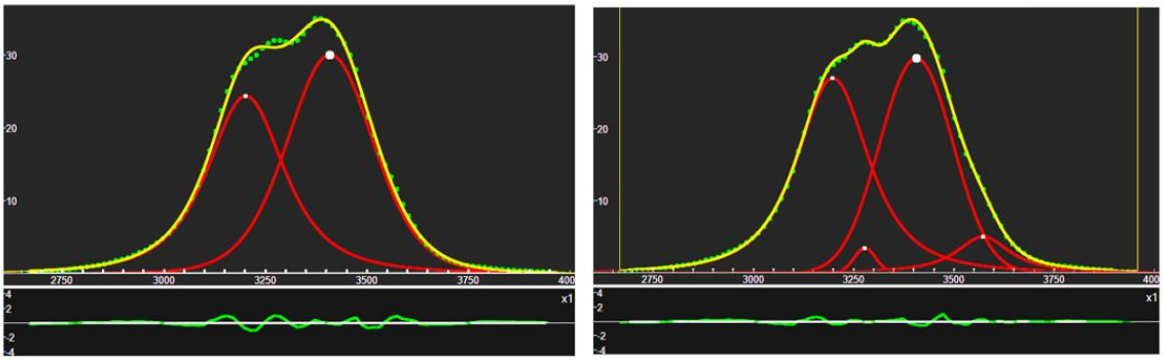

Fig.2: Increasing the number of components, the misfit, that is the different between data and sum of components, is reduced.

After these reminders about water, let us pass to consider the OH-stretching region of vivianite, and to the deconvolution of it. The Raman spectra that we consider are those kindly provided by RRUFF.

RRUFF database – The aim of the RRUFF Project is that of creating "a complete set of high-quality spectral data from well characterized minerals and is developing the technology to share this information with the world". Further information about the project in Lafuente et al., 2015. In RRUFF we can find several spectra of vivianite and a spectrum of baricite and a spectrum of bobierrite. To decompose them, we will use the q-Gaussians. For what is regarding the number of components, since from literature we identify five band as in our Table II, let us try deconvolutions with five components.

Vivianite R060035. RRUFF ID: R060025, Ideal Chemistry: $Fe^{2+}_3(PO_4)_2{\cdot}8H_2O$. Locality: Gypsy mine, Minas Gerais, Brazil. Source: Eric Van Valkenburg. Owner: RRUFF. Description: Blue-green fragment. Status: The identification of this mineral has been confirmed by X-ray diffraction. Broad scan on unoriented sample. Instrument settings: Thermo Almega XR 532nm @ 100% of 150mW. We use the processed data, in the range from 2000 to 4000 cm^{-1}. A spline baseline adjustment is applied. The deconvolution is given in the Figure 3.

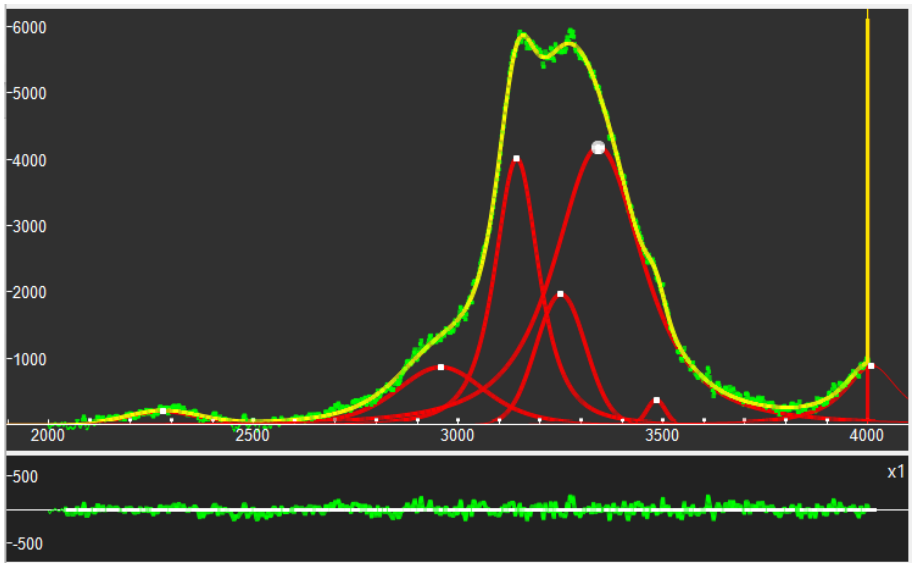

Fig.3: Deconvolution of vivianite RRUFF R060025 spectrum. The OH-stretching region is decomposed into five q-Gaussian bands. The centers of the components are at 2957, 3143, 3250, 3342, 3483 cm^{-1}.

Vivianite R050596. RRUFF ID: R050596. Locality: Chernomorskiy Quarry, near Kertch City, Crimea Peninsula, Ukraine. Source: Barb Dutrow. Owner: RRUFF. Description: Group of dark blue elongated prismatic single crystals in a fossilized clam shell. Status: The identification of this mineral has been confirmed by X-ray diffraction and chemical analysis. Sample Description: Microprobe Fragment, Measured Chemistry: $(Fe^{2+}_{2.89}Mg_{0.08}Mn_{0.03})_{\Sigma=3}(P_{1.00}O_4)_2{\cdot}8H_2O$. Sample Description: Unoriented sample, Instrument settings: Thermo Almega XR 532nm @ 100% of 150mW. We use the processed data, in the range from 2000 to 4000 cm^{-1}. A spline baseline adjustment is applied. The deconvolution is given in the Figure 4.

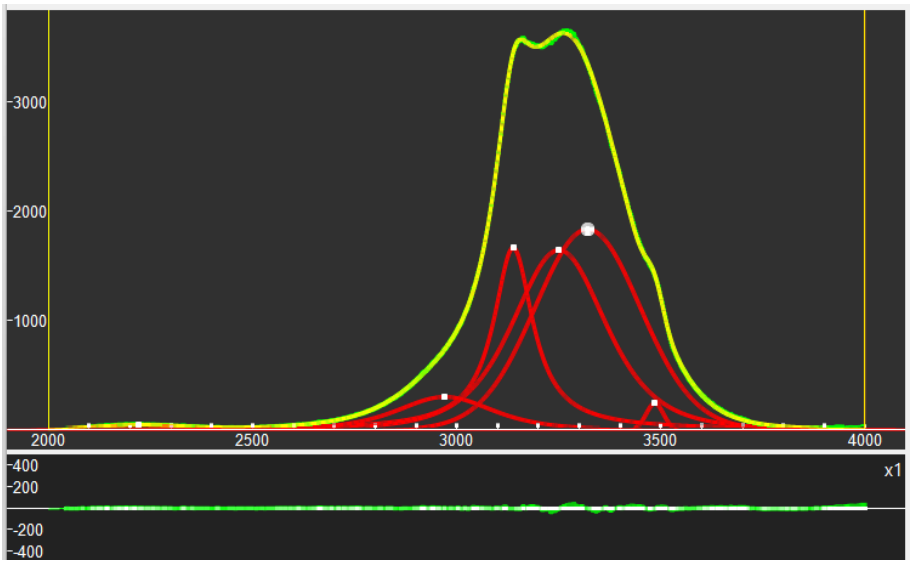

Fig.4: Deconvolution of vivianite RRUFF R050596 spectrum. As in the previous figure, the OH-stretching region is decomposed into five q-Gaussian bands. The centers of the components are at 2971, 3138, 3250, 3320, 3485 cm^{-1}.

Vivianite R050464. Locality: Siglo XX mine, Llallagua, Potosi, Bolivia. Source: University of Arizona Mineral Museum 11555. Owner: RRUFF. Description: Bluish green elongated prismatic crystals. Status: The identification of this mineral is confirmed by single-crystal X-ray diffraction and chemical analysis. Sample Description: Microprobe Fragment. Measured Chemistry: $Fe^{2+}_{3.00}(P_{1.00}O_4)_2{\cdot}8H_2O$. Sample Description: Unoriented sample, Instrument settings: Thermo Almega XR 532nm @ 100% of 150mW. We use the processed data, in the range from 2000 to 4000 cm^{-1}. A spline baseline adjustment is applied. The deconvolution is given in the Figure 5.

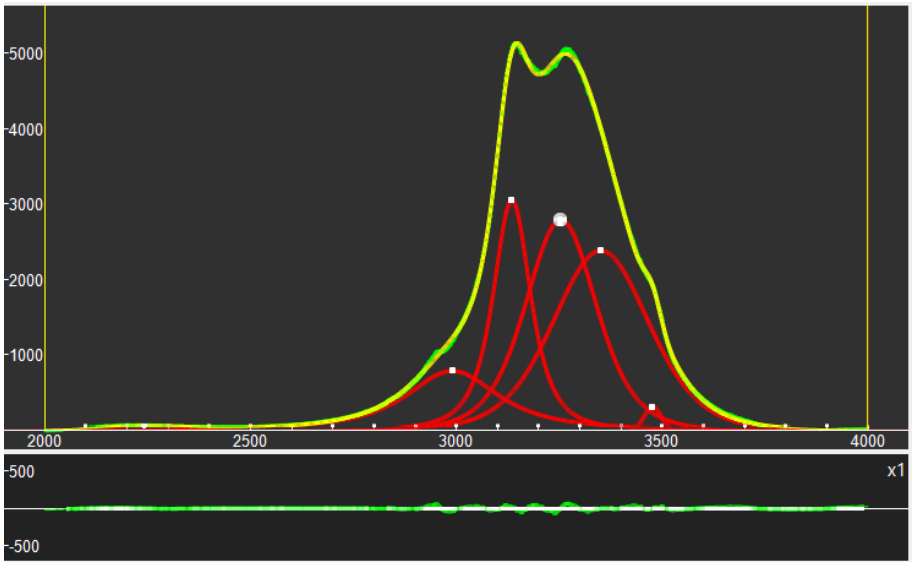

Fig.5: Deconvolution of vivianite RRUFF R050464 spectrum. The centers of the components are at 2990, 3135, 3254, 3351, 3477 cm^{-1}.

Vivianite R050076. Locality: near Canutillos mine, Potosi, Saavedra, Bolivia. Source: Rock Currier. Owner: RRUFF. Description: Green prismatic and elongated single crystal. Status: The identification of this mineral has been confirmed by X-ray diffraction and chemical analysis. Sample Description: Microprobe Fragment. Measured Chemistry: $Fe^{2+}_{0.99}Mn_{0.01})_3(P_{1.00}O_4)_2{\cdot}8H_2O$. Sample Description: Unoriented sample, Instrument settings: Thermo Almega XR 532nm @ 100% of 150mW. We use the

raw data, in the range from 2000 to 4000 cm^{-1}. A spline baseline adjustment is applied. The deconvolution is given in the Figure 6.

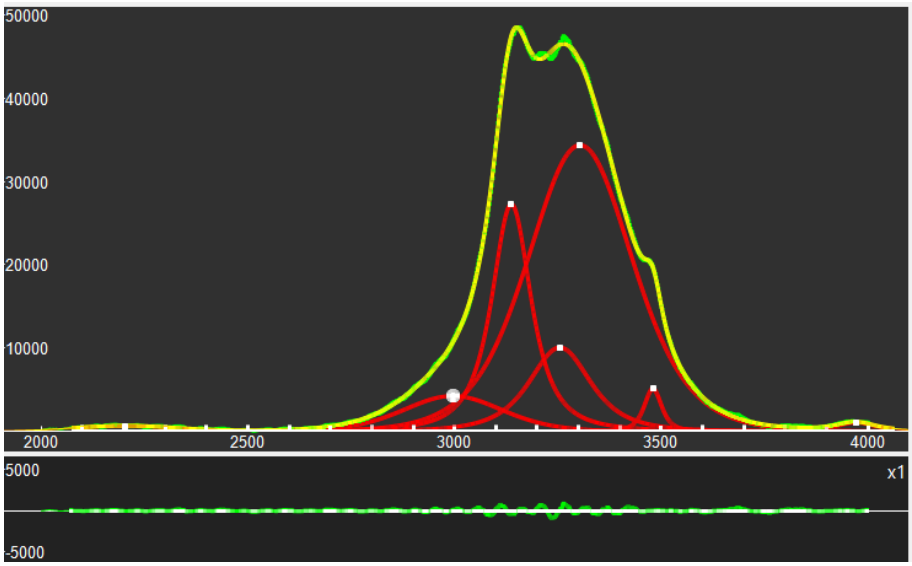

Fig.6: Deconvolution of vivianite RRUFF R050076 spectrum. The centers of the components are at 2996, 3137, 3254, 3303, 3480 cm^{-1}.

Vivianite R040185. Locality: Siglo XX mine, Llallagua, Bustillos, Potosi, Bolivia. Source: University of Arizona Mineral Museum 11555. Owner: RRUFF. Description: Green acicular single crystal. Status: The identification of this mineral has been confirmed by X-ray diffraction and chemical analysis. Microprobe Fragment. Measured Chemistry: $(Fe_{1.00}Mn_{0.01})_3(P_{0.97}Si_{0.03}O_{3.94}F_{0.07})_2 \cdot 8H_2O$. Unoriented sample. Instrument settings:Thermo Almega XR 532nm @ 100% of 150mW. We use the raw data, in the range from 2000 to 4000 cm^{-1}. A spline baseline adjustment is applied. The deconvolution is given in the Figure 7.

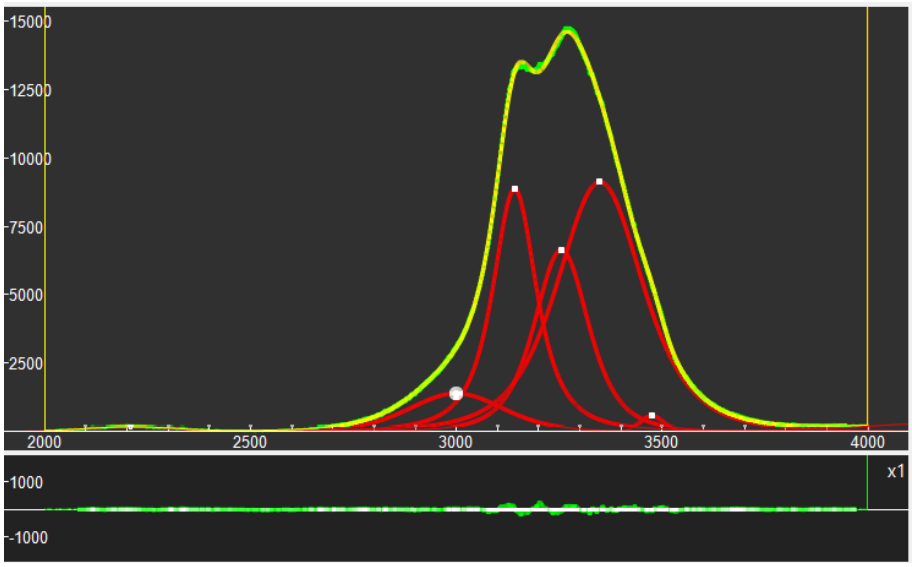

Fig.7: Deconvolution of vivianite RRUFF R040185 spectrum. The centers of the components are at 3000, 3141, 3255, 3349, 3475 cm^{-1}.

Vivianite R070331. Locality: Big Fish River, Yukon Territory, Canada. Source: Mark Mauthner 3369. Owner: RRUFF. Description: Platy, indigo-blue massive, associated with maricite. Status: The identification of this mineral is confirmed by single-crystal X-ray diffraction and chemical analysis.

Measured Chemistry: $(Fe^{2+}_{1.77}Mg_{1.21}Mn_{0.02})_{\Sigma=3}(P_{1.00}O_4)_2 \cdot 8H_2O$; (dark phase, H_2O is estimated by difference) : $Na_{1.00}Fe^{2+}_{1.00}P_{1.00}O_4$ (light phase = maricite, with trace amounts of Mn). Unoriented sample. Instrument settings: Thermo Almega XR 532nm @ 100% of 150mW. We use the raw data, in the range from 2000 to 4000 cm^{-1}. A spline baseline adjustment is applied. The deconvolution is given in the Figure 8.

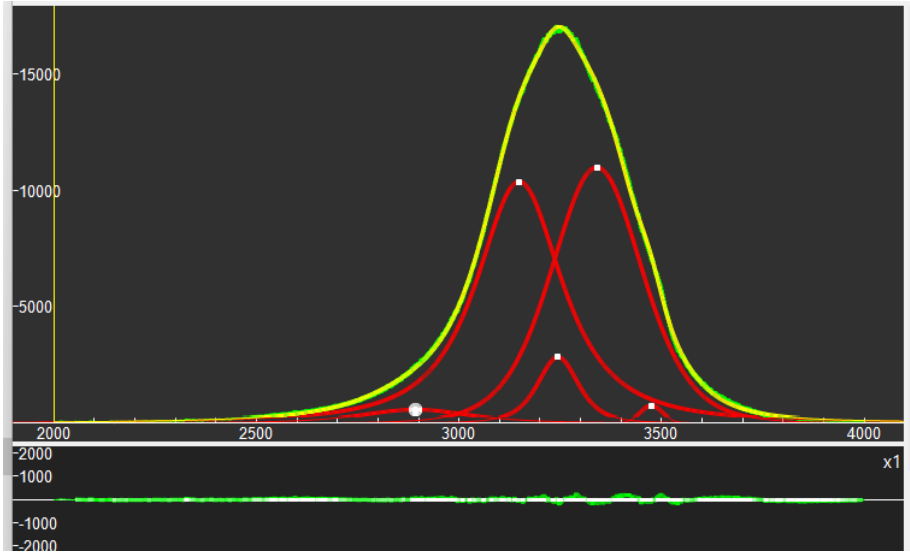

Fig.8: Deconvolution of vivianite RRUFF R070331 spectrum. The centers of the components are at 2892, 3148, 3244, 3340, 3475 cm^{-1}.

Barićite R061045. Ideal Chemistry: $(Mg,Fe)_3(PO_4)_2 \cdot 8H_2O$. Locality: Rapid Creek, Yukon, Canada. Source: Michael Scott S100392. Owner: RRUFF. Description: Bluish-gray translucent fragment. Status: The identification of this mineral is confirmed by single-crystal X-ray diffraction and chemical analysis. Microprobe Fragment. Measured Chemistry: $(Mg_{1.66}Fe_{1.33}Mn_{0.01})_{\Sigma=3}(P_{1.00}O_4)_2 \cdot 8H_2O$; H_2O estimated by difference. Unoriented sample. Instrument settings:Thermo Almega XR 532nm @ 100% of 150mW. We use the raw data, in the range from 2000 to 4000 cm^{-1}. A spline baseline adjustment is applied. The deconvolution is given in the Figure 9.

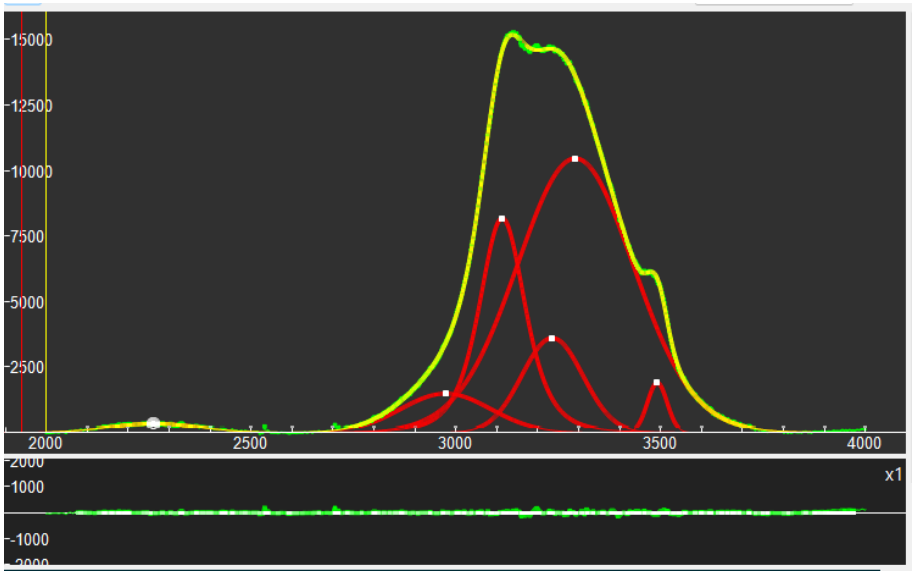

Fig.9: Deconvolution of baricite RRUFF R061045 spectrum. The centers of the components are at 2975, 3113, 3236, 3292, 3492 cm^{-1}.

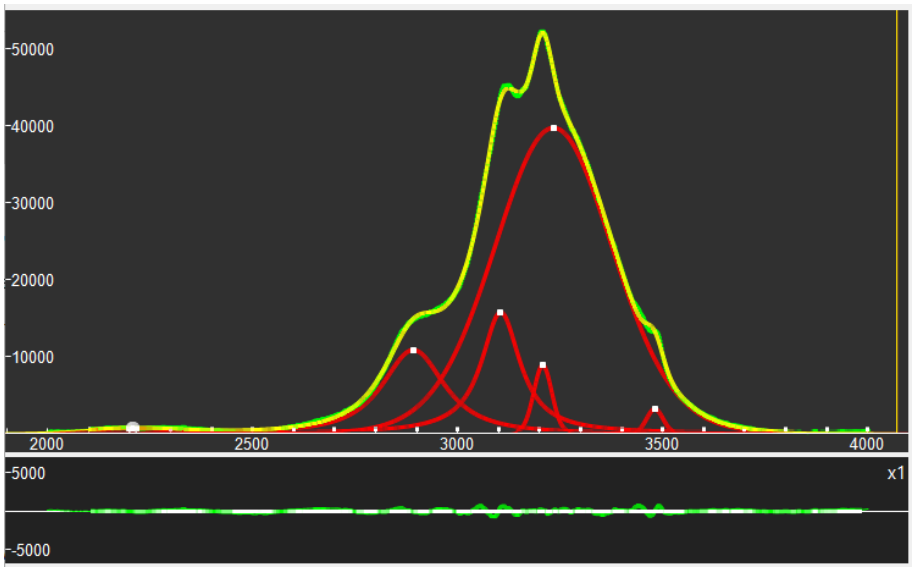

Fig.10: Deconvolution of bobierrite RRUFF R060681 spectrum. The centers of the components are at 2892, 3105, 3207, 3233, 3481 cm^{-1}.

Bobierrite R060681. Ideal Chemistry: $Mg_3(PO_4)_2 \cdot 8H_2O$. Locality: Kovdor Massif, Kola Peninsula, Murmanskaja Oblast', Northern Region, Russia. Source: Michael Scott S101377. Owner: RRUFF. Description: Colorless sectile tabular crystals. Status: The identification of this mineral has been confirmed by X-ray diffraction and chemical analysis. Microprobe Fragment. Measured Chemistry: $(Mg_{2.94}Fe_{0.05}Mn_{0.01})_{\Sigma=3}(P_{1.00}O_4)_2 \cdot 8H_2O$; H_2O estimated by difference. Unoriented sample. Instrument settings: Thermo Almega XR 532nm @ 100% of 150mW. We use the raw data, in the range from 2000 to 4000 cm^{-1}. A spline baseline adjustment is applied. The deconvolution is given in the Figure 10.

In the following Table III, we add the results from RRUFF samples (in cm^{-1}) to those given in the Table II.

Table III (centers of the bands, cm^{-1})

R060025	2957	3143	3250	3342	3483
R050596	2971	3138	3250	3320	3485
R050464	2990	3135	3254	3351	3477
R050076	2996	3137	3254	3303	3480
R040185	3000	3141	3255	3349	3475
R070331	2892	3148	3244	3340	3475
Chernomorskiy(a)		3137	3268		3487
Blackbird Dist		3131	3247		3473, 3486
Huanuni(a)		3131	3242, 3270, 3272		3480
Monserrat	2958	3133	3262		3478
Chernomorskiy(b)	3031	3137	3253	3351	3493
Huanuni(b)	3010	3135	3257	3391	
Vivianite (2002)	3012	3130	3263		3482, 3496
Ogorodova et al.		3138	3280		3475

Let us also add to the data of baricite and bobierrite in the Table I the results we obtained on RRUFF samples. The comparison is given in the Table IV.

Table IV (centers of the bands)

Baricite R061045	2975	3113	3236	3292	3492
Baricite (Frost et al.)	3025	3121	3231	3300	3480
Bobierrite R060681	2892	3105	3207	3233	3481
Bobierrite (Frost et al.)	2895	3096	3212	3263	3498

Discussion – From the Table III and IV, it seems that agreement exists among data. Then, one could ask why to use q-Gaussian functions instead of Gauss-Lorentz cross-product functions. Good reasons exist. First, as we have previously told, the q-parameter of the q-Gaussian is linked to the local environment of the oscillator.s This parameter allows the function to assume a shape ranging from Gaussian to Lorentzian. Moreover, what is a Gauss-Lorentz cross product function? We have an expression of it given by Origin. There is the shape parameter s; when s is equal to 1, we have a Lorentzian function.

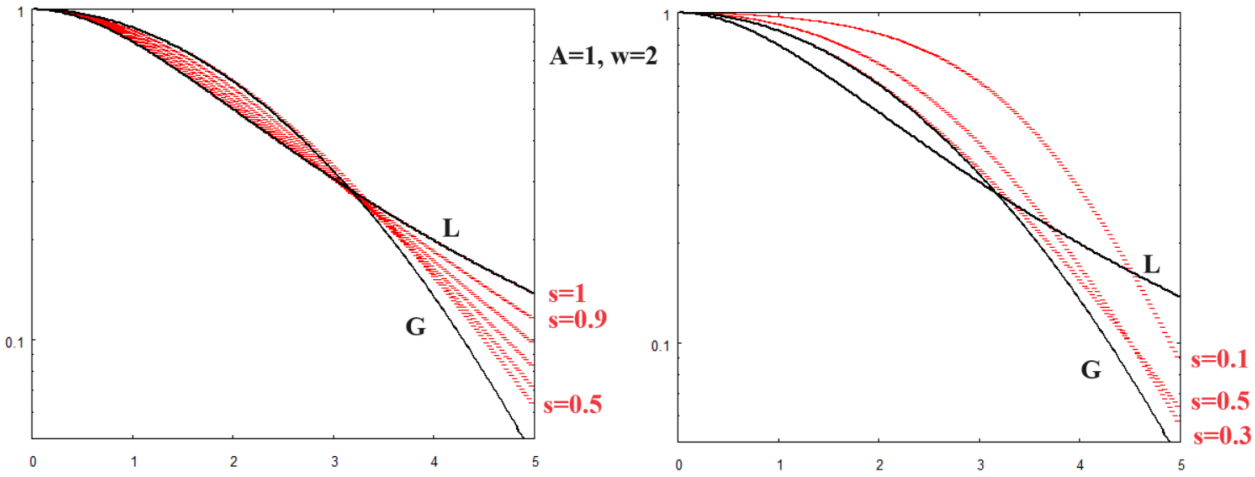

Fig.11: Behavior of the Gauss-Lorentz cross product function as given by Origin, in semilogarithmic scale, with the shape parameter varying from 0.1 to 1. Curve L and G are the Lorentzian and Gaussian functions.

Given the behavior of the Gauss-Lorentz cross product function as in the Fig.11, it is clear why Frost et al. used shape parameter greater than 0.7. It is also clear that a Gaussian shape can be never obtained. Then, let us consider a further Table V, where we show, besides the centers of the band, also their q-parameters.

Table V (centers and q-parameters of the q-Gaussian bands)

R060025	2957, 1.30	3143, 1.59	3250, 0.999	3342, 1.64	3483, 1.001
R050596	2971, 1.41	3138, 2.06	3250, 1.40	3320, 1.05	3485, 0.999
R050464	2990, 1.75	3135, 1.61	3254, 1.31	3351, 1.22	3477, 0.999
R050076	2996, 1.18	3137, 1.68	3254, 1.53	3303, 1.25	3480, 1.56
R040185	3000, 1.21	3141, 1.65	3255, 1.45	3349, 1.42	3475, 0.999
R070331	2892, 1.49	3148, 1.74	3244, 1.47	3340, 1.25	3475, 0.999

The Table V tells us that bands which are far from being Lorentzian are present. This is a good reason for using q-Gaussians, instead of Gauss-Lorentz cross product functions.

Appendix – q-Gaussian functions

The q-Gaussian functions are probability distributions proper of the Tsallis statistics (Tsallis, 1988, Hanel et al., 2009). These functions are based on a generalized form of the exponential function, characterized by a continuous real parameter q. When q is going to 1, the q-exponential becomes the usual exponential function. The value q=2, (Naudts, 2009), corresponds to the Cauchy distribution, also known as the Lorentzian distribution; the q-Gaussian function is therefore a generalization of the Lorentzian distribution too. The change of q-parameter is allowing the q-Gaussian function to pass from the Gaussian to the Lorentzian distribution. Sparavigna, 2023, proposed for the first time the use of q-Gaussian function in Raman spectroscopy.

As given by Umarov et al., 2008, the q-Gaussian function is: $f(x) = Ce_q(-\beta x^2)$, where $e_q(.)$ is the q-exponential function and C a scale constant (in the exponent, $\beta = 1/(2\sigma^2)$). The q-exponential has expression: $e_q(u) = [1 + (1-q)u]^{1/(1-q)}$.

In Fityk software, a q-Gaussian function can be defined in the following manner:

define Qgau(height, center, hwhm, q=1.5) = height*(1+(q-1)*((x-center)/hwhm)^2)^(1/(1-q))

q=1.5 the initial guessed value of the q-parameter. Parameter hwhm is the half width at half maximum of the component. When q=2, the q-Gaussian is a Lorentzian function, that we can find defined in Fityk as:

Lorentzian(height, center, hwhm) = height/(1+((x-center)/hwhm)^2)

When q is close to 1, the q-Gaussian becomes a Gaussian function.

References

1. Carey, D. M., & Korenowski, G. M. (1998). Measurement of the Raman spectrum of liquid water. The Journal of Chemical Physics, 108(7), 2669–2675, https://doi.org/10.1063/1.475659
2. Chaplin, M. (2022). Water structure and science, London South Bank University, https://water.lsbu.ac.uk/water/water_vibrational_spectrum.html

3. Chen, T., Song, X., & Xing, M. (2023). Study on anaerobic phosphorus release from pig manure and phosphorus recovery by vivianite method. Scientific Reports, 13(1), 16095.
4. Đuričković, I., Claverie, R., Bourson, P., Marchetti, M., Chassot, J. M., & Fontana, M. D. (2011). Water–ice phase transition probed by Raman spectroscopy. Journal of Raman Spectroscopy, 42(6), 1408-1412.
5. Frisenda, R., Niu, Y., Gant, P., Muñoz, M., & Castellanos-Gomez, A. (2020). Naturally occurring van der Waals materials. npj 2D Materials and Applications, 4(1), 38.
6. Frost, R. L., Martens, W., Williams, P. A., & Kloprogge, J. T. (2002). Raman and infrared spectroscopic study of the vivianite-group phosphates vivianite, baricite and bobierrite. Mineralogical Magazine, 66(6), 1063-1073.
7. Frost, R., & Weier, M. (2004). Raman spectroscopic study of vivianites of different origins. Neues Jahrbuch fur Mineralogie, Abhandlungen, 10, 445-463.
8. Gallo, P., Amann-Winkel, K., Angell, C.A., Anisimov, M.A., Caupin, F., Chakravarty, C., Lascaris, E., Loerting, T., Panagiotopoulos, A.Z., Russo, J., & Sellberg, J.A. (2016). Water: A tale of two liquids. Chemical reviews, 116(13), pp.7463-7500.
9. Hanel, R., Thurner, S., & Tsallis, C. (2009). Limit distributions of scale-invariant probabilistic models of correlated random variables with the q-Gaussian as an explicit example. The European Physical Journal B, 72(2), 263.
10. He, Z., Chang, J., Feng, Y., Wang, S., Yuan, Q., Liang, D., Liu, J. and Li, N., 2022. Carbon nanotubes accelerates the bio-induced vivianite formation. Science of The Total Environment, 844, p.157060.
11. Kappler, A., & Newman, D. K. (2004). Formation of Fe(III)-minerals by Fe(II)-oxidizing photoautotrophic bacteria. Geochim. Cosmochim. Ac. 68, 1217–1226. https://doi.org/10.1016/j.gca.2003.09.006
12. Lafuente, B., Downs, R. T., Yang, H., & Stone, N. (2015). 1. The power of databases: The RRUFF project. In Highlights in mineralogical crystallography (pp. 1-30). De Gruyter (O).
13. Li, S., Quhe, R., Weng, M., Feng, Y., Zuo, Y., Xiao, W., Zheng, J., Lu, J, & Pan, F. (2016). Few-layer Fe3 (PO4) 2· 8H2O: novel H-bonded 2D material and its abnormal electronic properties. The Journal of Physical Chemistry C, 120(46), pp.26278-26283.
14. Liu, J., Cheng, X., Qi, X., Li, N., Tian, J., Qiu, B., Xu, K., & Qu, D. (2018). Recovery of phosphate from aqueous solutions via vivianite crystallization: Thermodynamics and influence of pH. Chemical Engineering Journal, 349, pp.37-46.
15. Lu, S., Zeng, W., Gong, Q., Zhang, J., Peng, X., Yu, X., & Peng, Y. (2024). Anaerobic recovery of vivianite from waste-activated sludge through combined sludge pre-fermentation and agroforestry biomass-based biochar. Process Safety and Environmental Protection.
16. Miot, J., Benzerara, K., Morin, G., Kappler, A., Bernard, S., Obst, M., Férard, C., Skouri-Panet, F., Guigner, J.M., Posth, N., & Galvez, M. (2009). Iron biomineralization by anaerobic neutrophilic iron-oxidizing bacteria. Geochimica et Cosmochimica Acta, 73(3), pp.696-711.
17. Naudts, J. (2009). The q-exponential family in statistical physics. Central European Journal of Physics, 7, 405-413.
18. Ogorodova, L., Vigasina, M., Mel'chakova, L., Rusakov, V., Kosova, D., Ksenofontov, D., & Bryzgalov, I. (2017). Enthalpy of formation of natural hydrous iron phosphate: Vivianite. The Journal of Chemical Thermodynamics, 110, 193-200.
19. Paskin, A. (2024). Nucleation, Growth and Transformation Phenomena of Vivianite (Doctoral dissertation). Doctoral_Dissertation_FU_Berlin
20. Pinto, H. P., Michalkova, A., & Leszczynski, J. (2014). First-principles studies of paramagnetic vivianite Fe3 (PO4) 2· 8H2O surfaces. The Journal of Physical Chemistry C, 118(12), 6110-6121.

21. Pring, A. (1998). GAINES, RV, SKINNER, HCW, FOORD, EE, MASON, B. & ROSENZWEIG, A. 1997. Dana's New Mineralogy, xiv+ 1819 pp. New York, Chichester, Weinheim, Brisbane, Singapore, Toronto: John Wiley & Sons, Inc. Price£ 190.00 (hard covers). ISBN 0 471 19310 0. Geological Magazine, 135(5), 723-732.
22. Prot, T., Nguyen, V.H., Wilfert, P., Dugulan, A.I., Goubitz, K., De Ridder, D.J., Korving, L., Rem, P., Bouderbala, A., Witkamp, G.J., & Van Loosdrecht, M.C.M. (2019). Magnetic separation and characterization of vivianite from digested sewage sludge. Separation and Purification Technology, 224, pp.564-579.
23. Prot, T., Korving, L., Dugulan, A. I., Goubitz, K., & Van Loosdrecht, M. C. M. (2021). Vivianite scaling in wastewater treatment plants: Occurrence, formation mechanisms and mitigation solutions. Water Research, 197, 117045.
24. Rothe, M., Kleeberg, A., & Hupfer, M. (1026). The occurrence, identification and environmental relevance of vivianite in waterlogged soils and aquatic sediments. Earth-Sci. Rev. 158, 51–64. https://doi.org/10.1016/j.earscirev.2016.04.008
25. Silva, G. G., Vincenzi, R. A., de Araujo, G. G., Venceslau, S. J. S., & Rodrigues, F. (2024). Siderite and vivianite as energy sources for the extreme acidophilic bacterium Acidithiobacillus ferrooxidans in the context of mars habitability. Scientific Reports, 14(1), 14885.
26. Slomp, C.P. (2023). Vivianite blues. Nat. Geosci. 16, 394. https://doi.org/10.1038/s41561-023-01174-7
27. Sparavigna, A. C. (2023). q-Gaussian Tsallis Line Shapes and Raman Spectral Bands. Int. J. Sciences, 12(3), 27-40.
28. Sparavigna, A. C. (2023). q-Gaussian Tsallis Line Shapes for Raman Spectroscopy (June 7, 2023). SSRN Electronic Journal. http://dx.doi.org/10.2139/ssrn.4445044
29. Sparavigna A. C. (2023). Tsallis q-Gaussian function as fitting lineshape for Graphite Raman bands. ChemRxiv. Cambridge: Cambridge Open Engage; 2023.
30. Sparavigna, A. C. (2023). SERS Spectral Bands of LCysteine, Cysteamine and Homocysteine Fitted by Tsallis qGaussian Functions. International Journal of Sciences, 12(09), 14–24. https://doi.org/10.18483/ijsci.2721
31. Sparavigna, A. C. (2023). Multifunctional porosity in biochar. Int. J. Sciences, 7, 41-54. Available https://papers.ssrn.com/sol3/papers.cfm?abstract_id=4544693
32. Sparavigna, A. C. (2024). Kubo Lineshape and its Fitted q-Gaussian Tsallis Function. International Journal of Sciences, 13(01), 1-9.
33. Sparavigna, A. C. (2024). Water, q-Gaussians and Raman Spectroscopy. International Journal of Sciences, 13(03), 17-25. http://dx.doi.org/10.18483/ijSci.2751
34. Sparavigna, A. C. (2024). Applying q-Gaussians to the OH-stretching Raman bands of Water and Ice. International Journal of Sciences, 13(04), 1-10. http://dx.doi.org/10.18483/ijSci.2756
35. Tsallis, C. (1988). Possible generalization of Boltzmann-Gibbs statistics. Journal of statistical physics, 52, 479-487.
36. Umarov, S., Tsallis, C., Steinberg, S. (2008). On a q-Central Limit Theorem Consistent with Nonextensive Statistical Mechanics. Milan J. Math. Birkhauser Verlag. 76: 307–328. doi:10.1007/s00032-008-0087-y. S2CID 55967725.
37. Wang, Z., Pakoulev, A., Pang, Y., & Dlott, D. D. (2003). Vibrational substructure in the OH stretching band of water. Chemical physics letters, 378(3-4), 281-288.
38. Wang, S., An, J., Wan, Y., Du, Q., Wang, X., Cheng, X., Li, N. (2018). Phosphorus competition in bioinduced vivianite recovery from wastewater. Environmental science & technology, 52(23), pp.13863-13870.

39. Wang, P., Zuo, W., Zhu, W., Wang, S., Li, B., Jiang, Y., Wang, G., Tian, Y., & Zhang, Y. (2023). Deciphering the interaction of heavy metals with Geobacter-induced vivianite recovery from wastewater. Water Research, 245, p.120621.
40. Wilfert, P., Mandalidis, A., Dugulan, A.I., Goubitz, K., Korving, L., Temmink, H., Witkamp, G.J., & Van Loosdrecht, M.C.M. (2016). Vivianite as an important iron phosphate precipitate in sewage treatment plants. Water research, 104, pp.449-460.
41. Wilfert, P., Dugulan, A. I., Goubitz, K., Korving, L., Witkamp, G. J., & Van Loosdrecht, M. C. M. (2018). Vivianite as the main phosphate mineral in digested sewage sludge and its role for phosphate recovery. Water research, 144, 312-321.
42. Wojdyr, M. (2010). Fityk: a general-purpose peak fitting program. Journal of applied crystallography, 43(5), 1126-1128.
43. Wu, Y., Luo, J., Zhang, Q., Aleem, M., Fang, F., Xue, Z., & Cao, J. (2019). Potentials and challenges of phosphorus recovery as vivianite from wastewater: A review. Chemosphere, 226, 246-258.
44. Yang, X., Zhang, C., Zhang, X., Deng, S., Cheng, X., & Waite, T. D. (2023). Phosphate recovery from aqueous solutions via vivianite crystallization: Interference of FeII oxidation at different DO concentrations and pHs. Environmental Science & Technology, 57(5), 2105-2117.
45. Zhang, J., Chen, Z., Liu, Y., Wei, W., & Ni, B. J. (2022). Phosphorus recovery from wastewater and sewage sludge as vivianite. Journal of Cleaner Production, 370, 133439.
46. Zhao, L., Liu, L., Liu, X., Shu, A., Zou, W., Wang, Z., Zhou, Y., Huang, C., Zhai, Y. and He, H., 2024. Efficient phosphorus recovery from waste activated sludge: pretreatment with natural deep eutectic solvent and recovery as vivianite. Water Research, p.122161.